INTERNATIONAL JOURNAL FOR NUMERICAL METHODS IN FLUIDS, VOL. 18, 509–528 (1994)

ASPECTS OF THE TRANSPIRATION MODEL FOR AEROFOIL DESIGN

K. F. C. YIU

Oxford University Computing Laboratory, 11 Keble Road, Oxford OX1 3QD, U.K.

AND

P. STOW

Rolls-Royce plc, PO Box 31, Derby DE2 8BJ, U.K.

SUMMARY

Transpiration is a technique in which extra non-physical normal flows are created on an aerofoil surface in order to form a new streamline pattern such that the surface streamlines no longer follow the aerofoil surface under inviscid flow. The transpiration model is an important technique adopted in aerofoil design either to avoid mesh regeneration when aerofoil profile co-ordinates are adjusted or to find shape corrections in inverse design methods. A first-order approximation (with respect to the normal streamline displacement) to the transpiration model is commonly adopted; it is shown that this can be a poor approximation especially in regions of high curvature. In this paper more accurate approximations are developed to address this problem and improve the accuracy.

KEY WORDS Aerofoils Design Transpiration

1. INTRODUCTION

In this paper the use of a surface transpiration technique is reviewed. This technique is often adopted in computational fluid dynamics analysis of flow past aerofoils or turbomachinery blades to represent changes in the geometry without the need for mesh regeneration. In the model, transpiration of mass, momentum and energy through the surface is related to geometry changes. The technique is commonly used to represent the effects of a surface boundary layer on an inviscid flow and also in inverse design methods. In an inverse design problem the geometry of the aerofoil needs to be determined to optimize some requirements. Often this is achieved by specifying a target surface velocity distribution. In most approaches a sequence of profiles is constructed to approach the optimum through iterations. Since the aerofoil profile is modified after iteration, the use of a transpiration model avoids mesh regeneration that would otherwise be necessary. This technique has been used for turbomachinery blade design.[1] Apart from being used to simulate streamline movements, the transpiration model has also been used in calculating shape corrections in inverse design methods.[2,3]

In general, however, a first-order model is usually adopted. This is known to have limitations in regions of high curvature, e.g. leading edges. This problem is addressed in the current paper. A full transpiration model is formulated and simple examples are used to demonstrate the function of transpiration. Various approximations are discussed and numerical results are presented to illustrate their accuracy.

CCC 0271–2091/94/050509–20

Received December 1992
Revised October 1993

2. FORMULATION OF THE TRANSPIRATION MODEL

Suppose an initial aerofoil profile $\gamma(s)$ is given. Let the new aerofoil profile $\hat{\gamma}(s)$ be defined by (Figure 1)

$$\hat{\gamma}(s) = \gamma(s) + \xi(s)n(s), \quad s \in [0, s_n], \tag{1}$$

where $n(s)$ is the unit normal vector of $\gamma(s)$, $\xi(s)$ is the normal streamline displacement and s_n is the total arc length of $\gamma(s)$. Assume further that the trailing edge of $\hat{\gamma}$ is fixed such that $\xi(0) = \xi(s_n) = 0$. The flow field around $\hat{\gamma}(s)$ can be simulated by suitably transpiring fluid over $\gamma(s)$ so that the streamline pattern corresponds to the flow field around $\hat{\gamma}(s)$. The transpiration velocity $w_n(s)$ over $\gamma(s)$ is related to the tangential velocity component $w_s(s)$ and the normal displacement $\xi(s)$ through the conservation of mass. Consider the control volume in Figure 2 and write $m(s, n) = \rho w_s$; we have

$$\int_s^{s+\Delta s} \rho w_n \, ds = \int_0^{\xi(s+\Delta s)} m(s + \Delta s, n) \, dn - \int_0^{\xi(s)} m(s, n) \, dn. \tag{2}$$

Dividing both sides by Δs and taking the limit $\Delta s \to 0$,

$$\rho w_n = \frac{d}{ds} \int_0^{\xi(s)} m(s, n) \, dn. \tag{3}$$

Finally, using Leibnitz's rule of differentiation,

$$\rho w_n = \int_0^{\xi(s)} \frac{dm}{ds} \, dn + m(s, \xi)\xi'(s). \tag{4}$$

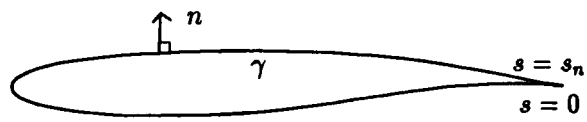

Figure 1. The parametrization

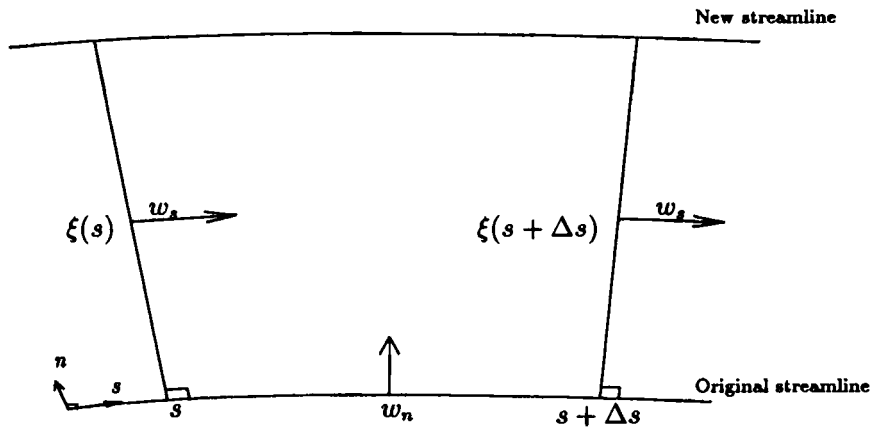

Figure 2. Control volume

It remains to show how to incorporate the transpiration velocity into the continuity equation. The continuity equation for steady flow is

$$\nabla \cdot (\rho \mathbf{u}) = 0, \tag{5}$$

where $\mathbf{u}$ is the velocity vector. For isentropic flow a velocity potential ϕ can be introduced such that

$$\nabla \phi = \mathbf{u}. \tag{6}$$

Because of the isentropic assumption, the energy equation can be integrated to give

$$\tfrac{1}{2}|\mathbf{u}|^2 + \frac{c^2}{\tilde{\gamma} - 1} = \text{constant}, \tag{7}$$

where $\tilde{\gamma}$ is the ratio of specific heats and c is the speed of sound. Using the isentropic relations (see e.g. Reference 4, p. 321)

$$p = \alpha \rho^{\tilde{\gamma}} \tag{8}$$

and

$$c^2 = \tilde{\gamma} p / \rho, \tag{9}$$

where α is a constant, (7)–(9) can be combined to give the relation

$$\rho = \rho(|\nabla \phi|). \tag{10}$$

As a result, substituting (6) into (5) and using (10), (5) finally becomes a non-linear differential equation for ϕ which is the so-called full potential equation. In order to solve the full potential equation for the flow field, it remains to impose suitable boundary conditions.

For aerofoil calculations the freestream velocity is imposed in the far field. On the aerofoil surface the transpiration velocity is imposed as a Neumann boundary condition. The final boundary value problem is posed as*

$$\nabla \cdot (\rho \nabla \phi) = 0 \quad \text{in } \Omega, \tag{11a}$$

$$\partial \phi / \partial n = w_n \quad \text{on } \gamma, \tag{11b}$$

$$\partial \phi / \partial n = \mathbf{u}_\infty \cdot \mathbf{n}_\infty \quad \text{on } \gamma_\infty, \tag{11c}$$

where Ω and γ_∞ are as defined in Figure 3 and $\mathbf{u}_\infty \cdot \mathbf{n}_\infty$ is a prescribed normal velocity on γ_∞. It can be rewritten using the weak formulation as

$$\int_\Omega \rho \nabla \phi \cdot \nabla N_i \, \mathrm{d}x = \int_\gamma \rho w_n N_i \, \mathrm{d}s + \int_{\gamma_\infty} \rho \frac{\partial \phi}{\partial n} N_i \, \mathrm{d}s \quad \forall N_i \in H^1(\Omega), \tag{12}$$

where $\{N_i\}$ denotes the test space and $H^1(\Omega)$ denotes the Sobolev space. For a given ξ (12) can be used to solve for ϕ. If $\xi = 0$, then from (4) $w_n = 0$ and it is equivalent to impose the flow tangency boundary condition on γ. Thus solving (12) for ϕ will give the flow field around γ. However, if ξ is not zero, (12) together with (4) can be solved for ϕ which corresponds to the

* For lifting flow calculations one extra variable and one extra equation are required in the formulation. The extra variable is the circulation which is used to generate lift, while the extra equation is known as the Kutta condition and equalizes the trailing edge velocities leaving the upper and the lower surface.

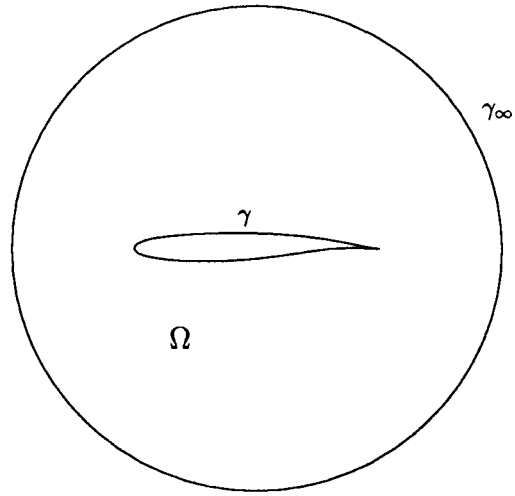

Figure 3. The computational domain for airfoils

flow field around $\hat{\gamma}$. As a demonstration, two simple examples using the incompressible non-lifting flow around a circle are used to illustrate how the transpiration velocity functions. Instead of (1), the family of circles is parametrized using cylindrical polar co-ordinates as

$$\hat{r}\begin{pmatrix}\cos\theta\\ \sin\theta\end{pmatrix} = r\begin{pmatrix}\cos\theta\\ \sin\theta\end{pmatrix} + \Delta r\begin{pmatrix}\cos\theta\\ \sin\theta\end{pmatrix}, \quad \theta \in [0, 2\pi]. \tag{13}$$

Denote C_r to be the circle with radius r and D_r to be the disc with radius r. Since the flow is assumed to be incompressible, the density ρ in (11) is equal to unity throughout. The first example is a profile expansion problem. Suppose we pose the boundary value problem as

$$\nabla^2\phi = 0 \quad \text{in } D_{0\cdot5}, \tag{14}$$

$$\partial\phi/\partial n = -3\cos\theta \quad \text{on } C_{0\cdot5}, \tag{15}$$

$$\phi \to r\cos\theta \quad \text{as } r \to \infty, \tag{16}$$

where the transpiration velocity on $C_{0\cdot5}$ is $w_n = -3\cos\theta$. This problem can be solved analytically and the solution is given by

$$\phi = (r + 1/r)\cos\theta. \tag{17}$$

Since the derivative

$$\partial\phi/\partial r = (1 - 1/r^2)\cos\theta \tag{18}$$

vanishes at $r = 1$, it implies that the unit circle is a streamline. Therefore the solution corresponds to the flow field around the unit circle. Equation (4) can easily be verified with $\xi = 0{\cdot}5$ in this case. The velocity vectors are shown in Figure 4. It can be observed that the transpiration velocity effectively creates flows around that circle $C_{0\cdot5}$ which interact with the freestream flow to form the streamline C_1.

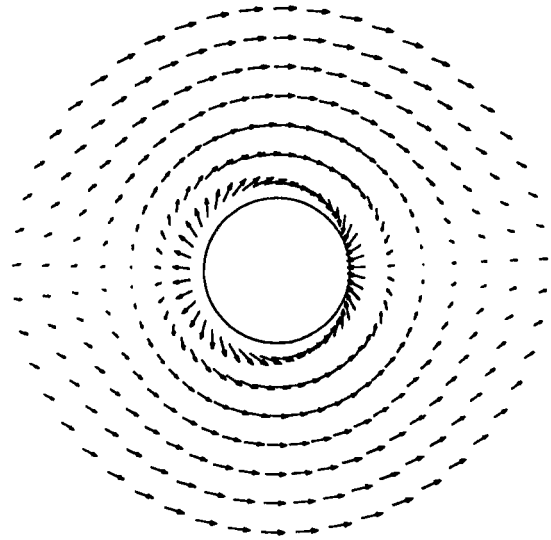

Figure 4. Example 1

The second example is a profile contraction problem. Suppose we pose the boundary value problem as

$$\nabla^2\phi = 0 \quad \text{in } D_1, \tag{19}$$

$$\partial\phi/\partial n = -0{\cdot}75\cos\theta \quad \text{on } C_1, \tag{20}$$

$$\phi \to r\cos\theta \quad \text{as } r \to \infty, \tag{21}$$

where the transpiration velocity on C_1 is $w_n = -0{\cdot}75\cos\theta$. The analytic solution of this problem is given by

$$\phi = (r + 1/4r)\cos\theta. \tag{22}$$

Since the derivative

$$\partial\phi/\partial r = (1 - 1/4r^2)\cos\theta \tag{23}$$

vanishes at $r = 0{\cdot}5$, it shows that the circle $C_{0{\cdot}5}$ is a streamline. Therefore the solution corresponds to the flow field around the circle $C_{0{\cdot}5}$. Equation (4) can easily be verified with $\xi = -0{\cdot}5$ in this case. The velocity vectors are shown in Figure 5. Here the transpiration velocity effectively creates continuations of the freestream flow inside the unit disc and forms the new streamline $C_{0{\cdot}5}$ inside D_1.

For compressible flows (12) must be used to solve for ϕ. In the analysis problem $\xi(s)$ is given and the co-ordinates of $\hat{\gamma}(s)$ can be calculated from (1). Therefore (12) together with (4) can be used to solve for ϕ. The tangential velocity distribution along $\hat{\gamma}$ is given by

$$\hat{w}_s \equiv \partial\phi/\partial s|_{\hat{\gamma}}, \tag{24}$$

where the subscript $\hat{\gamma}$ denotes evaluation along the displaced stream $\hat{\gamma}(s)$. On the other hand, in the inverse problem a target velocity distribution q_d is imposed on $\hat{\gamma}$ such that

$$\hat{w}_s = q_d \quad \text{on } \hat{\gamma}. \tag{25}$$

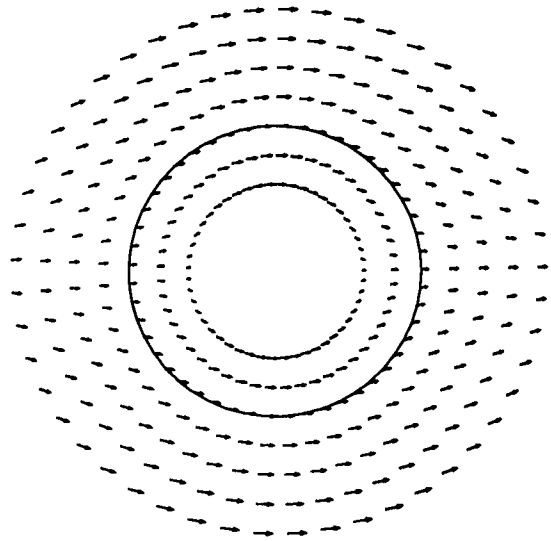

Figure 5. Example 2

The problem is to find $\xi(s)$ such that (25) is satisfied when (12) is solved. There are two main difficulties in trying to apply (4) and (24) for calculations. First of all, it is difficult to trace the new streamline $\hat{\gamma}(s)$ in the computational domain numerically. Thus it is difficult to evaluate $\hat{w}_s$ using (24). Secondly, ρw_n is defined by a line integral inside the domain of computation. After substitution into (12), the resulting equation is complicated and difficult to solve numerically. Therefore in the next section we shall describe some approximations to (4) and (24) so that the transpiration model can be applied practically.

3. APPROXIMATIONS OF THE MODEL

As discussed in the last section, the arbitrariness of the co-ordinates of $\hat{\gamma}$ causes a major problem in applying the transpiration model. One way to overcome this difficulty is to use Taylor's expansion about the fixed initial aerofoil profile γ to approximate all the terms which are not evaluated on γ. For (24) we have

$$\hat{w}_s = w_s + \frac{\partial w_s}{\partial n}\xi + \frac{1}{2}\frac{\partial^2 w_s}{\partial n^2}\xi^2 + O(\xi^3), \tag{26}$$

where the right-hand side is understood to be evaluated on γ. For (3) $m(s, n)$ is first expanded as

$$m(s, n) = m(s, 0) + \left.\frac{\partial m}{\partial n}\right|_{s,0} n + \left.\frac{1}{2}\frac{\partial^2 m}{\partial n^2} n^2\right|_{s,0} + O(n^3). \tag{27}$$

Substituting into (3) and integrating, using the definition of $m(s, n)$, we finally have

$$\rho w_n = \frac{\partial}{\partial s}\left(\rho w_s \xi + \frac{1}{2}\frac{\partial}{\partial n}(\rho w_s)\xi^2 + \frac{1}{6}\frac{\partial^2}{\partial n^2}(\rho w_s)\xi^3\right) + O(\xi^4) + O(\xi^3\xi'), \tag{28}$$

where $' \equiv \mathrm{d}/\mathrm{d}s$. In order to use the above approximations, the normal derivatives of w_s and ρw_s are required. These normal derivatives can be approximated by the tangential derivatives on γ via conservation laws. First of all, if γ is a streamline, we can derive the exact relations which are given by the following three lemmas.

Lemma 1

Under the isentropic assumption we have

$$\partial w_s/\partial n = -\kappa w_s, \tag{29}$$

$$\partial(\rho w_s)/\partial n = (M^2 - 1)\rho\kappa w_s, \tag{30}$$

where κ is the curvature of the aerofoil surface.

Proof. For flow over a two-dimensional curved surface the normal equilibrium equation is given by

$$\partial p/\partial n = \kappa\rho w_s^2, \tag{31}$$

where the right-hand side is the centrifugal force exerted on the fluid particles. Under the isentropic assumption we have (see e.g. Reference 4, p. 321)

$$p = \alpha\rho^{\tilde{\gamma}}, \tag{32}$$

$$c^2 = \tilde{\gamma}p/\rho, \tag{33}$$

where $\tilde{\gamma}$ is the ratio of the specific heats, c is the speed of sound and α is a constant. Substituting (32) into (31) gives

$$\tilde{\gamma}\alpha\rho^{\tilde{\gamma}-1}\frac{\partial\rho}{\partial n} = \kappa\rho w_s^2. \tag{34}$$

From (7) we have

$$w_s\,\mathrm{d}w_s + \frac{\mathrm{d}c^2}{\tilde{\gamma}-1} = 0. \tag{35}$$

Using (32) and (33),

$$\mathrm{d}\rho = \frac{\rho}{c^2}\frac{\mathrm{d}c^2}{\tilde{\gamma}-1} = -\frac{\rho}{c^2}w_s\,\mathrm{d}w_s. \tag{36}$$

Using (36) in (34),

$$-\frac{\tilde{\gamma}\alpha\rho^{\tilde{\gamma}}}{\rho c^2}\frac{\partial w_s}{\partial n} = \kappa w_s. \tag{37}$$

Finally, using (32) and (33) gives

$$\partial w_s/\partial n = -\kappa w_s. \tag{38}$$

To prove (30), notice that

$$\frac{\partial}{\partial n}(\rho w_s) = \rho \frac{\partial w_s}{\partial n} + w_s \frac{\partial \rho}{\partial n}. \tag{39}$$

Using (29) and (36), this becomes

$$\frac{\partial}{\partial n}(\rho w_s) = -\rho \kappa w_s - \frac{\rho}{c^2} w_s^2 \frac{\partial w_s}{\partial n} = (M^2 - 1)\rho \kappa w_s. \tag{40}$$

□

In order to get an even higher-order approximation, we need to calculate the second-order normal derivative. let the streamline γ_ε be defined by

$$\gamma_\varepsilon(s) = \gamma(s) - \varepsilon r(s) n(s), \tag{41}$$

where $n(s)$ is the normal vector of $\gamma(s)$ pointing inwardly. Because (29) is true along the streamline γ_ε in the flow field (Figure 6) for some $\varepsilon > 0$, the limit at poins s can be taken as

$$\frac{\partial^2 w_s}{\partial n^2} = \lim_{\varepsilon \to 0} \left(\frac{\partial w_s}{\partial n}(\gamma_\varepsilon) - \frac{\partial w_s}{\partial n}(\gamma) \right) \Big/ \varepsilon r = -\lim_{\varepsilon \to 0} \frac{\kappa(\gamma_\varepsilon) w_s(\gamma_\varepsilon) - \kappa(\gamma) w_s(\gamma)}{\varepsilon r} = -\frac{\partial}{\partial n}(\kappa w_s). \tag{42}$$

Thus the second-order normal derivative of w_s can be calculated as

$$\frac{\partial^2 w_s}{\partial n^2} = -\kappa \frac{\partial w_s}{\partial n} - w_s \frac{\partial \kappa}{\partial n} \tag{43}$$

and the problem reduces to calculating $\partial \kappa / \partial n$. In order to calculate the limit

$$\frac{\partial \kappa}{\partial n} = \lim_{\varepsilon \to 0} \frac{\kappa_\varepsilon - \kappa}{\varepsilon r}, \tag{44}$$

the actual structure of the streamline γ_ε must be considered. One way to visualize γ_ε is to apply the streamline curvature method[5,6] given by

$$\partial \psi / \partial n = \rho w_s. \tag{45}$$

We discretize and rearrange the terms to give

$$\Delta n = r \Delta \psi, \tag{46}$$

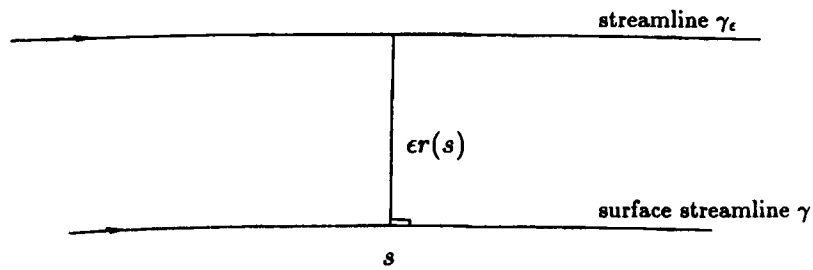

Figure 6. Streamlines off the surface streamline γ

where $r = 1/\rho w_s$. Taking $\Delta\psi = \varepsilon$, we then have the streamline

$$\gamma_\varepsilon(s) = \gamma(s) - \varepsilon r(s) n(s), \tag{47}$$

which is of the form of (41). As a result, κ_ε can be calculated and is given by the following lemma.

Lemma 2

Assume that $\gamma(s)$ is a positively oriented closed curve and is parametrized by its arc length $s \in [0, s_0]$. Let

$$\gamma_\varepsilon(s) = \gamma(s) - \varepsilon r(s) n(s), \quad s \in [0, s_0], \tag{48}$$

where $n(s)$ is the normal vector of $\gamma(s)$ pointing inwardly. Denote by $\kappa_\varepsilon(s)$ and $\kappa(s)$ the curvatures of $\gamma_\varepsilon(s)$ and $\gamma(s)$ respectively; then

$$\kappa_\varepsilon(s) = \kappa(s) - \varepsilon r(s)\kappa^2(s) - \varepsilon r''(s) + o(\varepsilon), \tag{49}$$

where $'' \equiv d^2/ds^2$ and the notation $o(\varepsilon)$ means $o(\varepsilon)/\varepsilon \to 0$ as $\varepsilon \to 0$.

Proof. The curvature of $\gamma_\varepsilon(s)$ is given by

$$\kappa_\varepsilon(s) = \sqrt{[(\gamma_\varepsilon' \cdot \gamma_\varepsilon')(\gamma_\varepsilon'' \cdot \gamma_\varepsilon'') - (\gamma_\varepsilon' \cdot \gamma_\varepsilon'')^2]} / \sqrt{[(\gamma_\varepsilon' \cdot \gamma_\varepsilon')^3]}. \tag{50}$$

The following relations in differential geometry for plane curves will be used:

$$\gamma' \cdot \gamma' = 1, \tag{51}$$

$$\gamma' \cdot n = 0, \tag{52}$$

$$n \cdot n = 1, \tag{53}$$

$$\gamma'' = \kappa n, \tag{54}$$

$$n' = -\kappa\gamma'. \tag{55}$$

The derivatives of γ_ε are given by

$$\gamma_\varepsilon' = (1 + \varepsilon r\kappa)\gamma' - \varepsilon r' n, \tag{56}$$

$$\gamma_\varepsilon'' = \varepsilon(2r'\kappa + r\kappa')\gamma' + (\kappa + \varepsilon r\kappa^2 - \varepsilon r'')n. \tag{57}$$

Therefore the inner products can be calculated as

$$\gamma_\varepsilon' \cdot \gamma_\varepsilon' = (1 + \varepsilon r\kappa)^2 + \varepsilon^2 r'^2, \tag{58}$$

$$\gamma_\varepsilon'' \cdot \gamma_\varepsilon'' = \varepsilon^2(2r'\kappa + r\kappa')^2 + (\kappa + \varepsilon r\kappa^2 - \varepsilon r'')^2, \tag{59}$$

$$\gamma_\varepsilon' \cdot \gamma_\varepsilon'' = \varepsilon(1 + \varepsilon r\kappa)(2r'\kappa + r\kappa') - \varepsilon r'(\kappa + \varepsilon r\kappa^2 - \varepsilon r''). \tag{60}$$

Hence

$$\begin{aligned}(\gamma_\varepsilon' \cdot \gamma_\varepsilon')(\gamma_\varepsilon'' \cdot \gamma_\varepsilon'') - (\gamma_\varepsilon' \cdot \gamma_\varepsilon'')^2 &= [1 + 2\varepsilon r\kappa + o(\varepsilon)][\kappa^2 + 2\varepsilon r\kappa^3 - 2\varepsilon r''\kappa + o(\varepsilon)] - o(\varepsilon) \\ &= \kappa^2(1 + 4\varepsilon r\kappa - 2\varepsilon r''/\kappa) + o(\varepsilon).\end{aligned} \tag{61}$$

Consequently

$$\kappa_\varepsilon = \kappa[1 + 4\varepsilon r\kappa - 2\varepsilon r''/\kappa + o(\varepsilon)]^{1/2}[1 + 2\varepsilon r\kappa + o(\varepsilon)]^{-3/2}$$
$$= \kappa(1 - \varepsilon r\kappa - \varepsilon r''/\kappa) + o(\varepsilon). \tag{62}$$

□

Using Lemma 2, the second-order normal derivatives can be calculated and are given by the following lemma.

Lemma 3

Using the streamline curvature method, we have

$$\partial\kappa/\partial n = -\kappa^2 - r''/r, \tag{63}$$

$$\frac{\partial^2 w_s}{\partial n^2} = 2\kappa^2 w_s + \frac{r''}{r} w_s, \tag{64}$$

$$\frac{\partial^2(\rho w_s)}{\partial n^2} = [(M^2 - 1)(M^2 - 2) - aM^2]\rho\kappa^2 w_s - (M^2 - 1)\rho\frac{r''}{r} w_s, \tag{65}$$

where $a = 2 + (\tilde{\gamma} - 1)M^2$.

Proof. From Lemma 2 we have

$$\frac{\partial\kappa}{\partial n} = \lim_{\varepsilon\to 0}\frac{\kappa_\varepsilon - \kappa}{\varepsilon r} = -\kappa^2 - \frac{r''}{r} + \lim_{\varepsilon\to 0}\frac{o(\varepsilon)}{\varepsilon r} = -\kappa^2 - \frac{r''}{r}. \tag{66}$$

To prove (64), notice that

$$\frac{\partial^2 w_s}{\partial n^2} = -\kappa\frac{\partial w_s}{\partial n} - w_s\frac{\partial\kappa}{\partial n} = 2\kappa^2 w_s + \frac{r''}{r} w_s. \tag{67}$$

Finally, to prove (65), we have

$$\frac{\partial^2(\rho w_s)}{\partial n^2} = (M^2 - 1)\left(\kappa\frac{\partial(\rho w_s)}{\partial n} + \rho w_s\frac{\partial\kappa}{\partial n}\right) + \rho\kappa w_s\frac{\partial M^2}{\partial n}. \tag{68}$$

It remains to find $\partial M^2/\partial n$. Taking the differentials on both sides of (7), we have

$$\frac{\mathrm{d}w_s^2}{2} + \frac{\mathrm{d}c^2}{\tilde{\gamma} - 1} = 0. \tag{69}$$

Therefore

$$\mathrm{d}M^2 = \mathrm{d}\left(\frac{w_s^2}{c^2}\right) = \frac{1}{c^2}\mathrm{d}w_s^2 - \frac{w_s^2}{c^2}\mathrm{d}c^2 = \frac{1}{c^2}\mathrm{d}w_s^2 + \frac{(\tilde{\gamma} - 1)M^2}{2c^2}\mathrm{d}w_s^2$$
$$= [2 + (\tilde{\gamma} - 1)M^2]\frac{w_s}{c^2}\mathrm{d}w_s \equiv a\frac{w_s}{c^2}\mathrm{d}w_s. \tag{70}$$

Substituting into (68), we finally have

$$\frac{\partial^2(\rho w_s)}{\partial n^2} = (M^2-1)\left[(M^2-1)\rho\kappa^2 w_s - \rho\kappa^2 w_s - \rho\frac{r''}{r}w_s\right] + a\rho\kappa\frac{w_s^2}{c^2}\frac{\partial w_s}{\partial n}$$

$$= [(M^2-1)(M^2-2) - aM^2]\rho\kappa^2 w_s - (M^2-1)\rho\frac{r''}{r}w_s. \tag{71}$$

□

Remark. If γ_ε is parallel to γ, then $r' = 0$ and (63) becomes

$$\partial\kappa/\partial n = -\kappa^2. \tag{72}$$

Thus the term r''/r can be interpreted as a correction term to the assumption that the streamlines γ_ε and γ are parallel.

Since the normal velocity component on γ is not zero when the transpiration velocity is applied, γ is no longer a streamline and the results derived in Lemmas 1 and 3 will not strictly hold. However, the results can still be used as approximations for the normal derivatives whenever the normal streamline displacement ξ is not too large. In numerical calculations the energy equation of the form

$$\tfrac{1}{2}w_s^2 + \frac{c^2}{\tilde{\gamma}-1} = \text{constant} \quad \text{on } \gamma \tag{73}$$

will be used, in which the contributions from w_n are neglected, and the density will be calculated as $\rho = \rho(w_s)$. We shall assess the accuracy of (29), (30) and (64), (65) in the next section by looking more closely at the error terms neglected in the approximations.

4. ERRORS IN THE APPROXIMATE MODELS

In proving Lemmas 1 and 3, the normal equilibrium equation (31) and the streamline curvature equation (45) are applied which are only true along a streamline. In this section more accurate conservation models will be applied to relate the normal derivatives with the tangential derivatives on γ without assuming γ to be a streamline. We summarize the results for the first-order normal derivatives in the following lemma.

Lemma 4

Under the isentropic assumption we have

$$\frac{\partial w_s}{\partial n} = -\kappa w_s + \frac{\partial w_n}{\partial s} \quad \text{on } \gamma, \tag{74}$$

$$\frac{\partial}{\partial n}(\rho w_s) = (M^2-1)\rho\kappa w_s + \rho\frac{\partial w_n}{\partial s} - \frac{\rho}{c^2}w_s\left(w_n\frac{\partial w_n}{\partial n} + w_s\frac{\partial w_n}{\partial s}\right) \quad \text{on } \gamma, \tag{75}$$

where κ is the curvature of γ.

Proof. The momentum equation in the normal direction is given by

$$\frac{\partial p}{\partial n} = \kappa \rho w_s^2 - \rho w_s \frac{\partial w_n}{\partial s} - \rho w_n \frac{\partial w_n}{\partial n}, \tag{76}$$

where $s - n$ are local co-ordinates based on γ (see Figure 2). Using (32) gives

$$\tilde{\gamma} \alpha \rho^{\tilde{\gamma}-1} \frac{\partial \rho}{\partial n} = \kappa \rho w_s^2 - \rho w_s \frac{\partial w_n}{\partial s} - \rho w_n \frac{\partial w_n}{\partial n}. \tag{77}$$

From (7) we have

$$w_s \, \mathrm{d}w_s + w_n \, \mathrm{d}w_n + \frac{\mathrm{d}c^2}{\tilde{\gamma} - 1} = 0. \tag{78}$$

Thus from (36) we have

$$\mathrm{d}\rho = -\frac{\rho}{c^2} w_s \, \mathrm{d}w_s - \frac{\rho}{c^2} w_n \, \mathrm{d}w_n. \tag{79}$$

Using this in (77) and after some manipulations gives

$$\partial w_s / \partial n = -\kappa w_s + \partial w_n / \partial s. \tag{80}$$

To prove (75), notice that

$$\frac{\partial}{\partial n}(\rho w_s) = \rho \frac{\partial w_s}{\partial n} + w_s \frac{\partial \rho}{\partial n}. \tag{81}$$

Using (74) and (79), this becomes

$$\begin{aligned} \frac{\partial}{\partial n}(\rho w_s) &= -\rho \kappa w_s + \rho \frac{\partial w_n}{\partial s} - \frac{\rho}{c^2} w_s^2 \frac{\partial w_s}{\partial n} - \frac{\rho}{c^2} w_s w_n \frac{\partial w_n}{\partial n} \\ &= (M^2 - 1)\rho \kappa w_s + \rho \frac{\partial w_n}{\partial s} - \frac{\rho}{c^2} w_s^2 \frac{\partial w_n}{\partial s} - \frac{\rho}{c^2} w_s w_n \frac{\partial w_n}{\partial n}. \end{aligned} \tag{82}$$

□

In deriving (64) and (65), the approximations (29) and (30) are used. Therefore (64) and (65) will inherit the errors in approximating $\partial w_s / \partial n$ and $\partial(\rho w_s)/\partial n$. Moreover, $\partial \kappa / \partial n$ is also used in the derivation. We shall assess the error in approximating $\partial \kappa / \partial n$ by (63) here. A less rigorous approach will be used. Consider (28) with a small transpiration mass ρw_n. Therefore terms of orders higher than one can be neglected and we have

$$\rho w_n = \frac{\partial}{\partial s}(\rho w_s \xi). \tag{83}$$

Integrating (83) gives

$$\xi(s) = \frac{1}{\rho w_s} \int_0^s \rho w_n \, \mathrm{d}s \tag{84}$$

$$\equiv \varepsilon(s) r(s), \tag{85}$$

where $r(s) = 1/\rho w_s$. Thus the new streamline $\hat{\gamma}$ is given by

$$\hat{\gamma}(s) = \gamma(s) - \varepsilon(s)r(s)n(s). \tag{86}$$

Comparing with (47), the only difference is that ε becomes a function of s here instead of a constant. By using the same argument used in proving Lemma 2, the curvature of $\hat{\gamma}(s)$ is given by

$$\kappa_\varepsilon = \kappa - \varepsilon r\kappa^2 - (\varepsilon r)'' + o(\|\varepsilon\|). \tag{87}$$

Therefore

$$\partial\kappa/\partial n \approx -\kappa^2 - (\varepsilon r)''/\varepsilon r \tag{88}$$

when $\|\varepsilon\|$ is sufficiently small. Comparing with (63), the key term $-\kappa^2$ is the same and the only difference comes from the second term.

As derived in Lemma 4, there are a few extra terms involving w_n that are not in (29) and (30). The same also applies to (64) and (65). However, those terms are not possible to be approximated accurately. Consequently, approximate models using the approximations (29), (30) and (64), (65) will be used throughout. In the next section we shall evaluate the approximate models numerically and demonstrate the accuracy of the models despite the neglected error terms.

5. EVALUATIONS OF THE APPROXIMATE MODELS

In this section we shall look at the performance of different approximate transpiration models with different truncations in (26) and (28). We shall predict the velocity distribution of a target profile via the mesh of an initial profile using these transpiration models and compare the results with the exact distribution which is generated by solving the full potential equation (12) on a new mesh around the target profile. The full potential equation is solved by the finite element method with piecewise linear trial and test functions. Denote:

model 1

$$\hat{w}_s = w_s, \tag{89a}$$

$$\rho w_n = \frac{\partial}{\partial s}(\rho w_s \xi); \tag{89b}$$

model 2

$$\hat{w}_s = (1 - \kappa\xi)w_s, \tag{90a}$$

$$\rho w_n = \frac{\partial}{\partial s}\{\rho w_s[\xi + \tfrac{1}{2}(M^2 - 1)\kappa\xi^2]\}; \tag{90b}$$

model 3

$$\hat{w}_s = (1 - \kappa\xi + \kappa^2\xi^2)w_s, \tag{91a}$$

$$\rho w_n = \frac{\partial}{\partial s}\{\rho w_s[\xi + \tfrac{1}{2}(M^2 - 1)\kappa\xi^2 + a_3\kappa^2\xi^3]\}, \tag{91b}$$

$$a_3 = \tfrac{1}{6}\{(M^2 - 1)(M^2 - 2) - M^2[2 + (\tilde{\gamma} - 1)M^2]\}. \tag{91c}$$

Note that the term r''/r is not included in model 3. This is because of the likely large truncation errors in estimating second-order derivatives with piecewise linear basis and test functions. Also, since the streamline curvature method has a singular point at the stagnation point, large numerical errors are likely to be incurred around the stagnation point and the approximation to $\partial\kappa/\partial n$ will not be so accurate. Thus the approximation

$$\partial\kappa/\partial n = 0 \quad \text{if } |w_s| < \delta \tag{92}$$

should be used, where δ is a small positive number. However, in the following test cases (92) is not needed.

The first example is subsonic non-lifting flow around a cylinder. The target profile is the cylinder $C_{1\cdot1}$ while the initial profile is the cylinder C_1. The results are depicted in Figures 7–9. We can see the improvement in accuracy with the increase in terms added.

The second example is subsonic non-lifting flow around an aerofoil. The initial aerofoil is the NACA 0012 and the target aerofoil (Figure 10) is generated as

$$\gamma^*(s) = \gamma(s) + \xi(s)n(s), \tag{93}$$

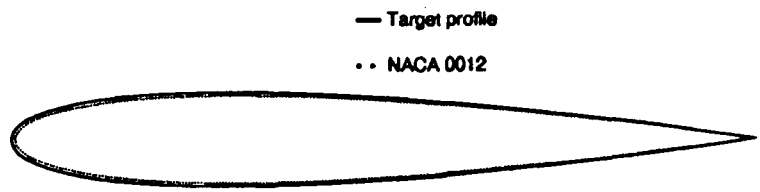

Figure 7. Model 1

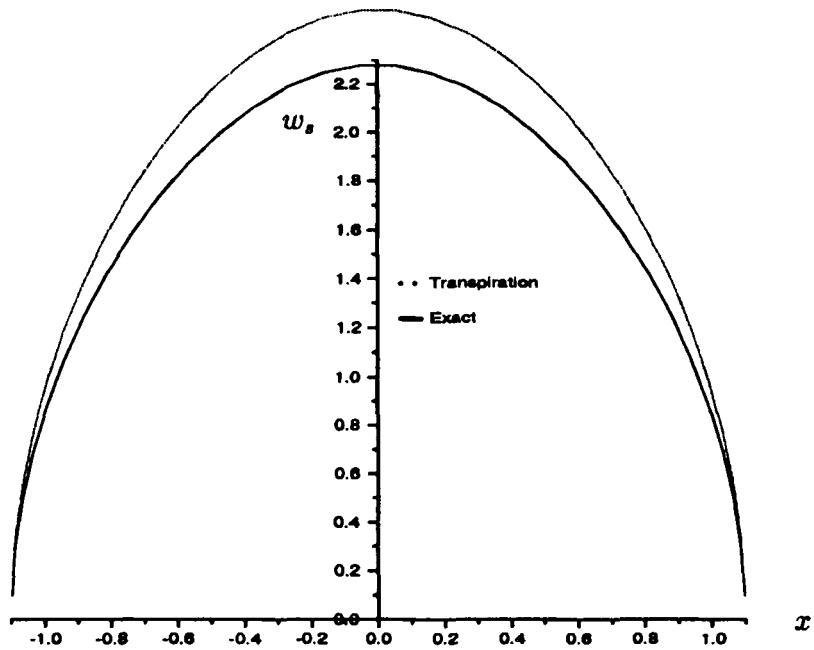

Figure 8. Model 2

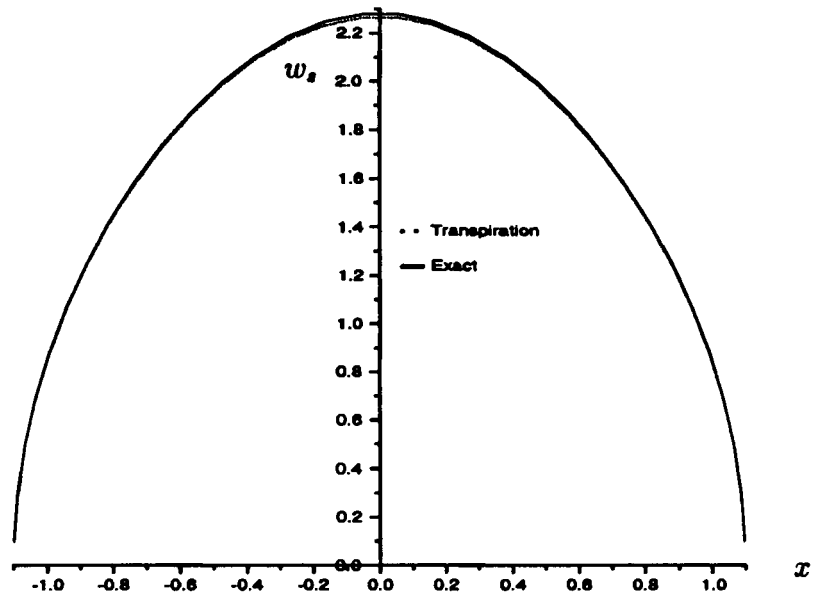

Figure 9. Model 3

where $\xi(s)$ is the function shown in Figure 11. After discretization, the aerofoil γ is approximated by a polygonal curve and the curvature is calculated approximately using the parametric cubic spline. Both ξ and κ are defined at nodal points; for simplicity, a linear interpolation is used to calculate the values at the midpoints of the elements whenever they are required. The results are shown in Figures 12–14. The curvature effect can be seen to be significant at the leading edge region. This accounts for the poor performance of model 1. Also, the accuracy is improved when model 3 is used.

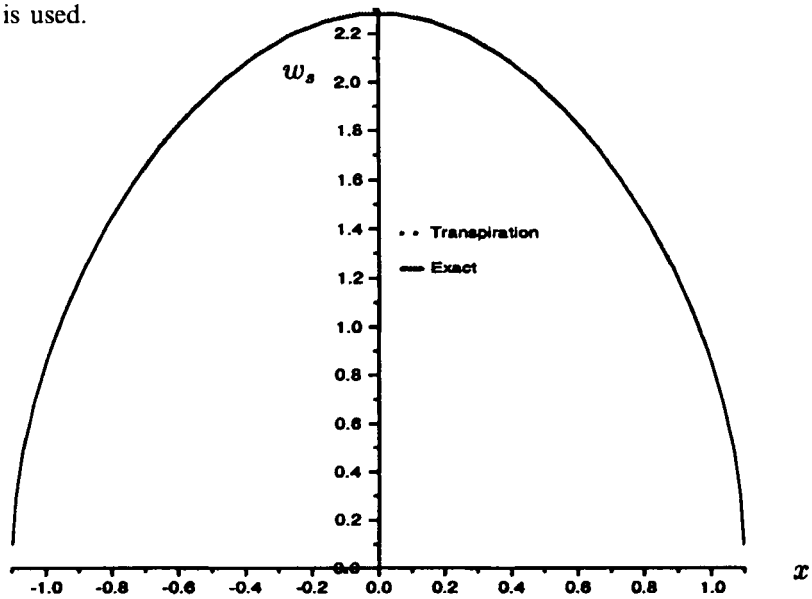

Figure 10. Iitial and target profiles

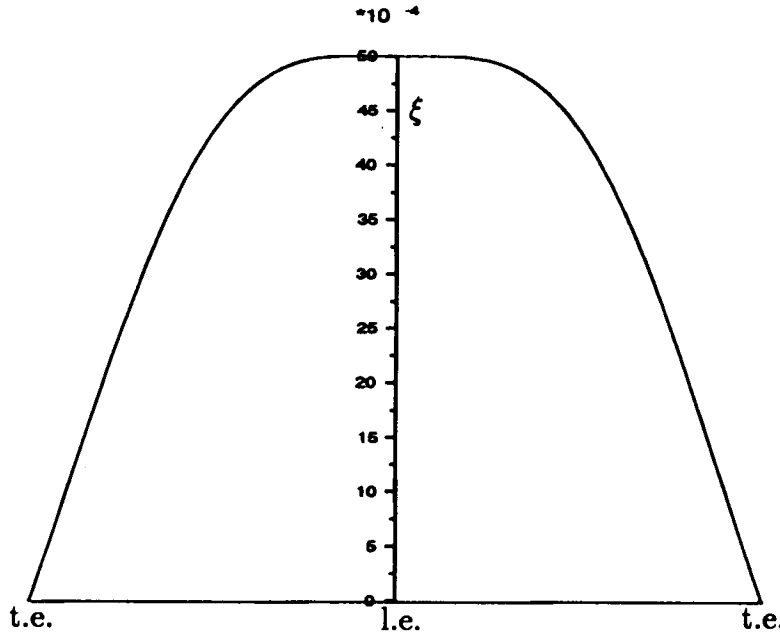

Figure 11. Distribution of ξ

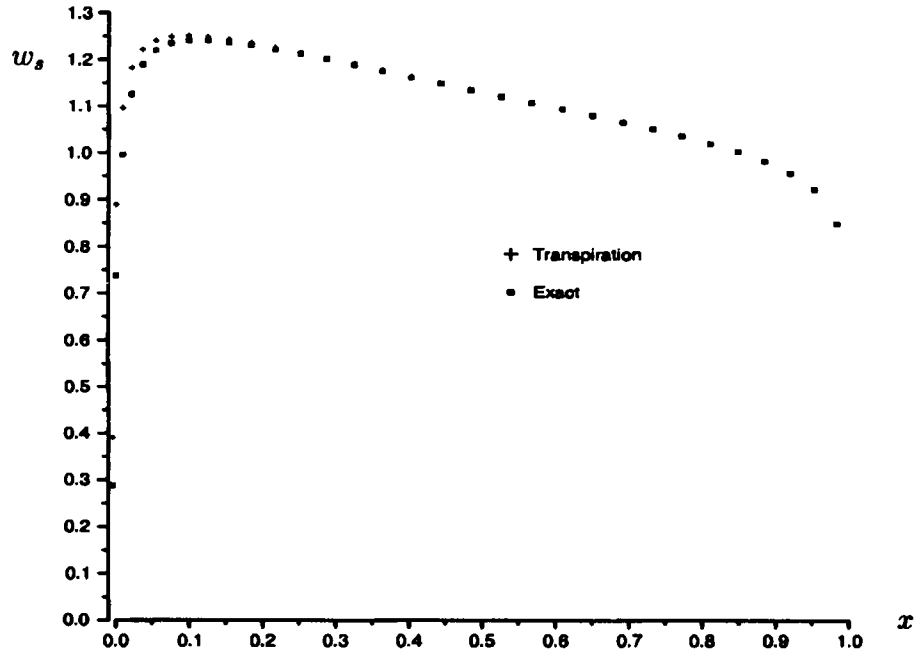

Figure 12. Model 1

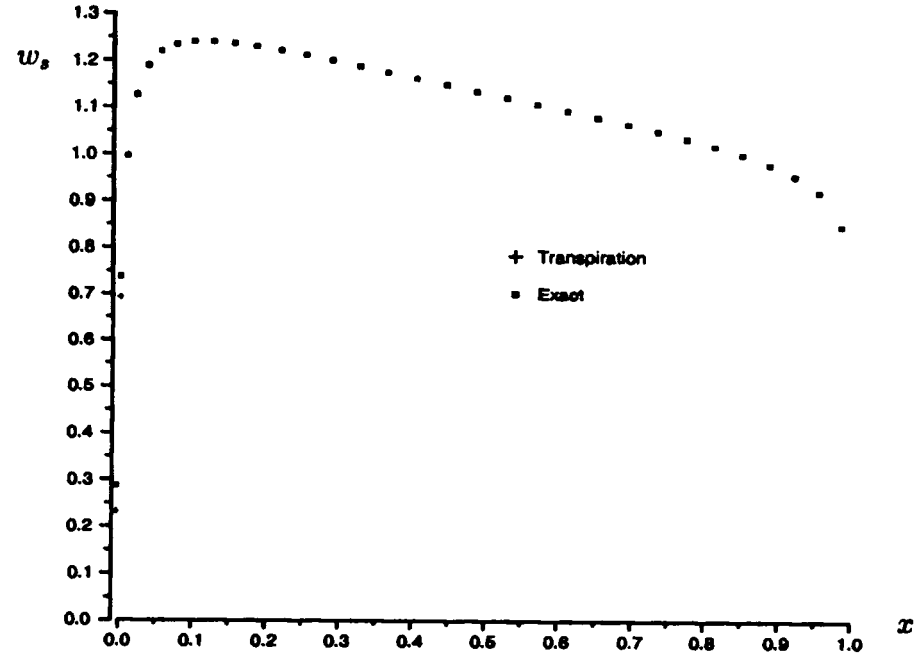

Figure 13. Model 2

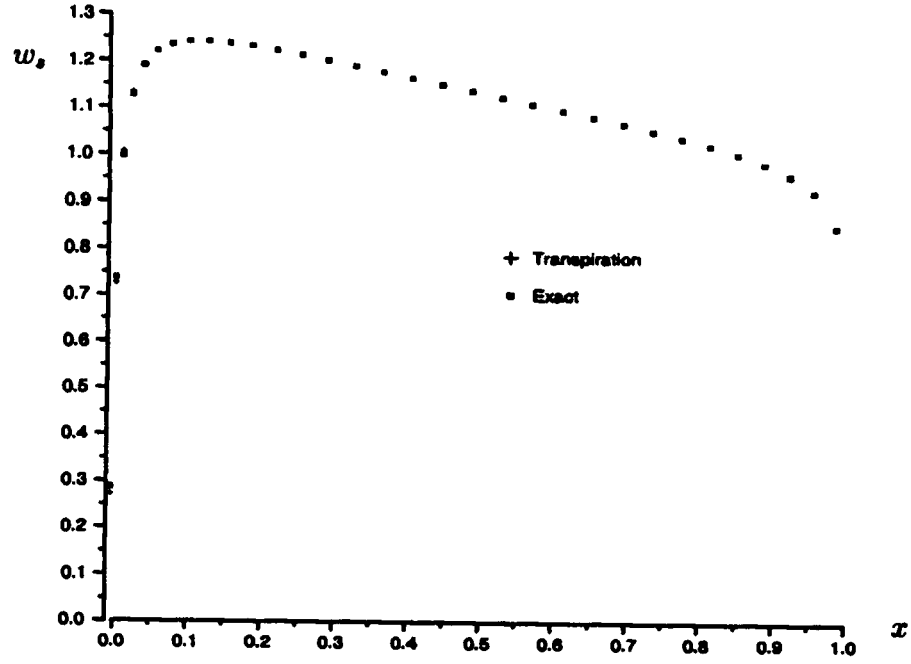

Figure 14. Model 3

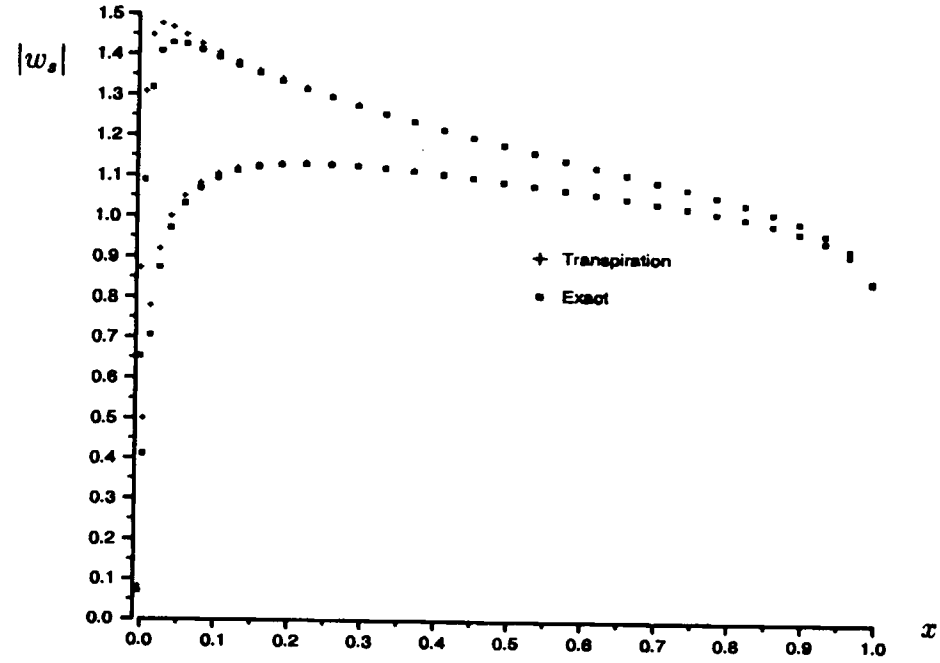

Figure 15. Model 1

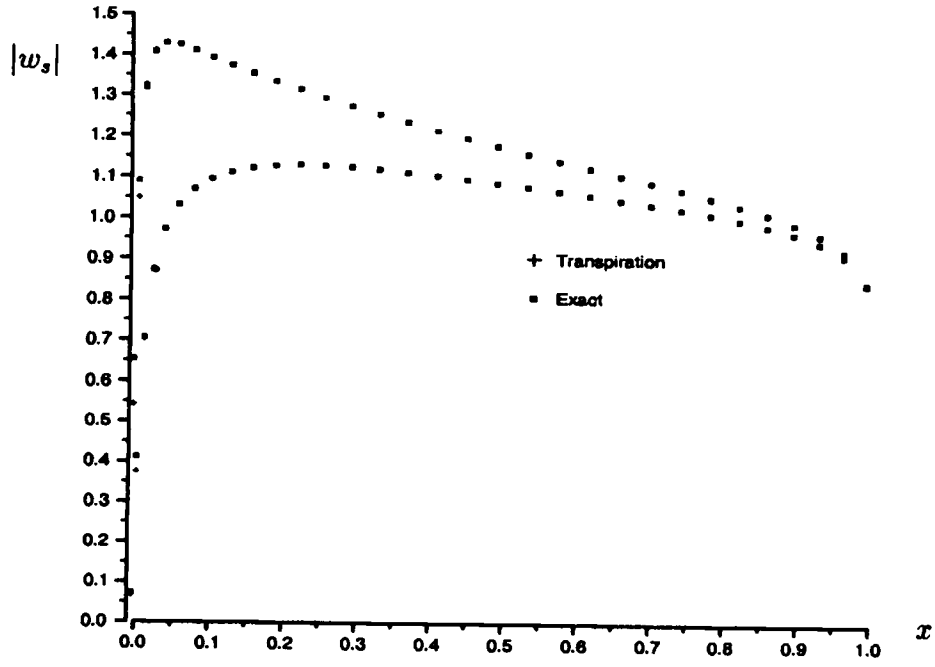

Figure 16. Model 2

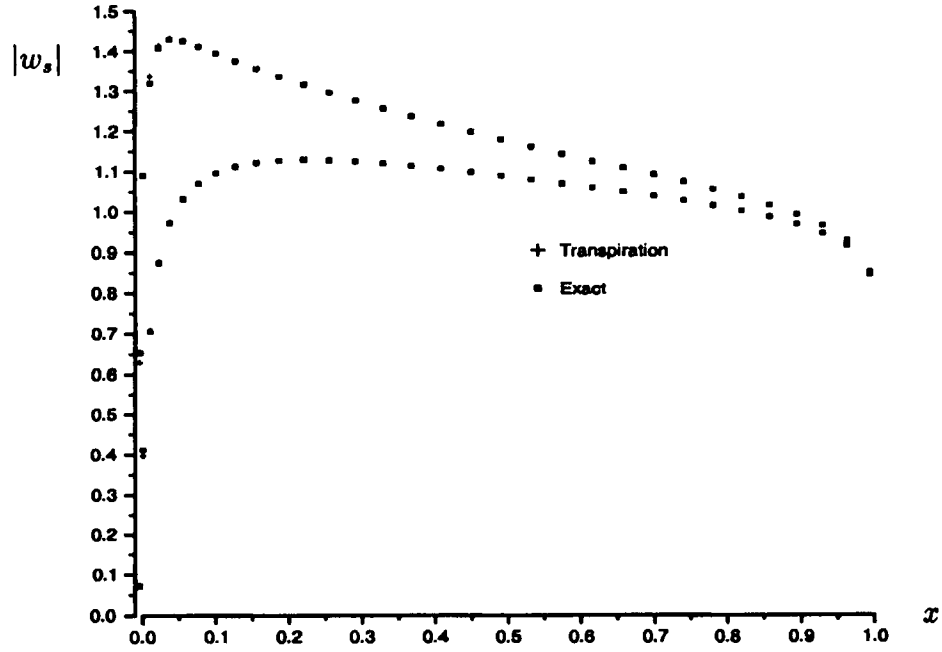

Figure 17. Model 3

The last example is subsonic lifting flow around an aerofoil. The initial and target aerofoils are the same as in the second example. The results can be found in Figures 15–17. Here the leading edge region is more sensitive. Similar conclusions can be drawn.

6. CONCLUDING REMARKS

The main aim of the paper has been to discuss various approximate forms of a surface transpiration model commonly used to represent changes in an aerofoil geometry without the need for mesh regeneration. Under the assumptions of isentropic flow, using the streamline curvature approach, approximations to the higher-order terms have been constructed. The superiority in accuracy in using the approximations and the limitations of the commonly adopted first-order method, especially in regions of high curvature, have been demonstrated with a number of examples.

The higher-order surface transpiration models introduce higher-order surface normal derivatives. In the method proposed these are related to surface tangential derivatives; these can be difficult to approximate accurately. It would be of interest to consider the merits of other approaches, e.g. the direct approximation of the normal derivatives provided by an orthogonal mesh and how this might be incorporated into a design algorithm.

ACKNOWLEDGEMENT

The authors wish to thank Professor K. W. Morton for his encouragement and fruitful discussions.

REFERENCES

1. R. D. Cedar and P. Stow, 'A compatible mixed design and analysis finite element method for the design of turbomachinery blades', *Int. J. Numer. Methods Fluids*, **5**, 331–345 (1985).
2. P. A. Henne, 'An inverse transonic wing design method', *AIAA Paper 80-0330*, 1980.
3. C. Nicoud, C. Le Bloa and O. P. Jacquotte, 'A finite element inverse method for the design of turbomachinery blades', *ASME Paper 91-GT-80*, 1991.
4. J. D. Anderson, *Fundamentals of Aerodynamics*, McGraw-Hill, New york, 1984.
5. W. Habashi, 'Numerical methods of turbomachinery', in C. Taylor and K. Morgan (eds), *Recent Advances in Numerical Methods in Fluids*, Vol. 1, Pineridge, Swansea, 1980, pp. 245–286.
6. J. P. Bindon and A. D. Carmichael, 'Streamline curvature analysis of compressible and high Mach number cascade flows', *J. Mech. Eng. Sci.*, **13**, 344–357 (1971).